Cloud Particle Phase Determination with the AVHRR

JEFFREY R. KEY

NOAA/National Environmental Satellite, Data, and Information Service, Madison, Wisconsin

JANET M. INTRIERI

NOAA/Environmental Technology Laboratory, Boulder, Colorado

30 April 1999 and 18 January 2000

ABSTRACT

An accurate determination of cloud particle phase is required for the retrieval of other cloud properties from satellite and for radiative flux calculations in climate models. The physical principles underlying phase determination using the advanced very high resolution radiometer (AVHRR) satellite sensor are described for daytime and nighttime, cold cloud and warm cloud conditions. It is demonstrated that the spectral properties of cloud particles provide necessary, but not sufficient, information for phase determination, because the relationship between the cloud and surface temperatures is also important. Algorithms based on these principles are presented and tested. Validation with lidar and aircraft data from two Arctic field experiments shows the procedures to be accurate in identifying the phase of homogeneous water and ice clouds, though optically thin, mixed-phase, and multilayer clouds are problematic.

1. Introduction

Cloud particle phase, size, and density determine to what degree radiation is absorbed, scattered, and transmitted. These physical properties are directly related to three important radiative (optical) properties: the single-scattering albedo, volume extinction coefficient, and phase function (cf. Slingo and Schrecker 1982). It is the optical properties that are used in radiative transfer models for the computation of upwelling and downwelling radiative fluxes and intensities. Therefore, the relationship between the microphysical and optical properties of clouds illuminates not only the need for estimates of phase, size, and density, but also the physical basis for how such estimates can be obtained from satellite measurements of upwelling radiation.

Determining the cloud particle phase, liquid or solid, is a prerequisite to estimating the particle size distribution and density. An incorrect phase assessment can lead to errors in estimates of the other properties, which, in turn, create uncertainties in estimates of radiative fluxes. For example, applying the methods described in Key (1999) to summertime, subarctic and Arctic advanced very high resolution radiometer (AVHRR) data, an incorrect determination of cloud phase can result in errors of 20%–100% in the retrieval of particle effective radius r_e (the ratio of the third to the second moments of the particle size distribution) and optical depth for scenes with approximately equal amounts of liquid and solid phase clouds. Those retrieval errors translate into errors in the calculated downwelling shortwave and longwave fluxes of 5%–20%.

Methods have been developed for the retrieval of cloud particle phase from the AVHRR on-board the National Oceanic and Atmospheric Administration (NOAA) polar-orbiting satellites. Arking and Childs (1985) use the visible (0.6 μm), solar infrared (3.7 μm), and thermal infrared (11 μm) channels of the AVHRR to determine a ''microphysical index'' that includes phase. Giraud et al. (1997) retrieve cloud-top temperature and a microphysical index of cirrus clouds from AVHRR data by clustering visible and thermal radiances and their local standard deviations. The reflectance at 3.7 μm was used in addition to the visible and thermal channel radiances of the AVHRR by Hutchison et al. (1997a) to distinguish cirrus cloud from snow in daytime imagery in the western United States. The International Satellite Cloud Climatology Project (ISCCP), which utilizes geostationary satellites and polar orbiters, determines phase based only on temperature in its D1 (three-hourly) and D2 (monthly) datasets; if the low- or middle-cloud temperature is less than 260 K then it is an ice cloud, otherwise it is liquid; high clouds are always ice clouds (Rossow et al. 1996).

Corresponding author address: Dr. Jeffrey R. Key, NOAA/NESDIS, 1225 W. Dayton St., Madison, WI 53706.
E-mail: jkey@ssec.wisc.edu

Methods have also been developed using thermal channels of the high-resolution infrared sounder (HIRS) instrument on the NOAA polar orbiters. Strabala et al. (1994) describe the theory and application of 8-, 11-, and 12-μm brightness temperatures and brightness temperature differences for particle phase determination. These wavelengths can be used day or night. Baum et al. (1994) examine nighttime data over the ocean using both AVHRR and HIRS, where the HIRS radiances provide information on cloud height, including multiple layers, and the AVHRR data provide information on other cloud properties. Hutchison et al. (1997b) use HIRS to resolve the ambiguity in their daytime phase analyses with the AVHRR, distinguishing between low-level water clouds and thin cirrus based on the estimated cloud-top pressure.

The purposes of this note are to discuss the physical principles underlying cloud phase determination with the AVHRR for both daytime and nighttime applications over a broad range of conditions, and to present procedures that can be applied to the more than two decades of AVHRR data. The theory described in Strabala et al. (1994) needs to be clarified in the context of the AVHRR because the 8-μm HIRS channel is not available on the AVHRR. In addition, the previous AVHRR studies were for either daytime or nighttime, and both the AVHRR and HIRS studies dealt with the more typical ''cold cloud'' situation where the surface temperature is higher than that of the cloud. In contrast, the methods presented here were initially developed for the polar regions where the surface is often colder than the cloud (''warm clouds''). The methods presented are limited, however, in that all clouds are considered to be composed of either liquid droplets (''water cloud'') or solid ice crystals (''ice cloud''), and no attempt is made to identify mixed-phase or multilayer clouds.

2. Physical principles

The determination of cloud particle phase is based on both physical and radiative properties. Physically, liquid cloud droplets can exist at temperatures as low as -40°C (e.g., Heymsfield et al. 1991), although clouds are likely to be composed of both liquid droplets and ice crystals at temperatures below -10°C. Radiatively, the spectral difference between water and ice clouds occurs because of differences in absorption and scattering. Figure 1 illustrates the absorption differences, showing the imaginary index of refraction for liquid and solid water. Because the imaginary index of refraction represents the absorptive properties of a material, it is clear from the figure that ice is a stronger absorber than water at the three AVHRR thermal channel wavelengths (3.7-, 11-, and 12-μm for channel numbers 3, 4, and 5, respectively), and that both ice and water are better absorbers at 11 and 12 μm than at 3.7 μm. Based only on the imaginary index of refraction, more absorption will take place in ice clouds at 11 and 12 μm than in water clouds,

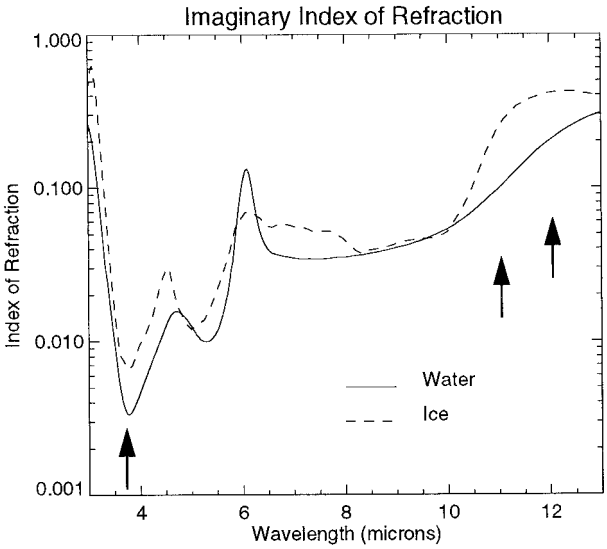

FIG. 1. Imaginary index of refraction for water and ice from 3 to 13 μm. The three arrows correspond to the three AVHRR thermal channels (3.7, 11, and 12 μm).

so brightness temperature differences between 3.7 and 11 μm will be larger for ice clouds. The same relationship exists for 8 μm as for 3.7 μm, and this is the basis for phase retrieval using HIRS (e.g., Strabala et al. 1994).

However, absorption alone does not explain observed spectral differences. The radiance measured at the satellite is a function not just of absorption–emission, but also of scattering and transmission. The single-scattering albedo ω indicates the degree of effectiveness of particles at scattering incident radiation. Unlike the imaginary index of refraction, it applies to a size distribution of particles. Figure 2 shows ω of water and ice clouds for four different r_e calculated with Mie theory for spherical particles. The figure illustrates that scattering is greater at 3.7 μm than at 11 or 12 μm. This complements the principle of stronger absorption at the longer wavelengths. The figure also shows that the smaller the particle, the greater the scattering, and that for typical ice crystal sizes there is very little difference in scattering across this portion of the spectrum. Furthermore, ω indicates that during the day ice clouds will exhibit a lower reflectance at 3.7 μm than water droplets. At visible wavelengths, ω of both water and ice clouds is near unity and absorption is near zero. However, ω is as much a function of particle size as of particle phase, so that retrieval algorithms utilizing ω are relying in part on the fact that water droplets are typically smaller than ice crystals. Much of the discussion below makes this assumption, though its effect on the algorithms presented is minimal.

a. Nighttime

For optically thick clouds where the transmittance is low and the surface contribution to the top of the at-

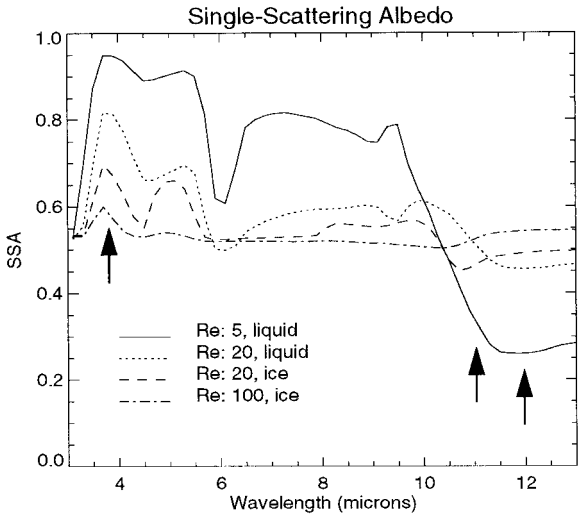

FIG. 2. Single-scattering albedo of liquid and ice clouds for effective radii (Re) of 5–100 μm over the three AVHRR thermal channels.

mosphere (TOA) radiance is small, absorption and scattering define the spectral characteristics of a cloud. Based on the principles presented above we expect the nighttime brightness temperature difference between channels 3 and 4, $T_3 - T_4$, to be negative for thick water clouds with small r_e. For thick ice clouds ω indicates that $T_3 - T_4$ would be smaller than for thick water clouds, and would be near zero for large ice particles. This is, in fact, the case, as demonstrated by the model calculations presented in Fig. 3. The model used is Streamer (Key and Schweiger 1998), which employs a discrete-ordinates solver. These nighttime calculations were done using eight streams and cloud optical properties for spherical particles. A snow surface was used with a surface emissivity of 0.99 for all channels.

For optically thin clouds the transmissivity is not negligible so the surface and lower portion of the cloud influence the brightness temperature measured at the satellite, particularly at 3.7 μm. Figure 3 illustrates this, where $T_3 - T_4$ for cold (surface is warmer than the cloud) clouds increases when the optical depth is small. The opposite occurs for warm clouds, where $T_3 - T_4$ can be negative. The relationships shown in Fig. 3 are similar to those presented in Yamanouchi et al. [(1987) their Figs. 3 and 4 for water and ice clouds] and Stone et al. [(1990) their Fig. 2b for ice clouds], but also include the warm cloud cases.

The spectral variation in surface emissivity for surface types other than snow will affect the brightness temperature differences for thin clouds; for example, for a sandy soil $T_3 - T_4$ will be reduced. However, the surface emissivity does not affect the phase detection algorithm described below, because thin clouds are not considered in the brightness temperature difference tests. Similarly, variations in water vapor will affect $T_3 - T_4$ but not the phase detection procedure.

The brightness temperature difference between 11 and 12 μm, $T_4 - T_5$, is much smaller than $T_3 - T_4$ for both water and ice clouds, and there is considerable overlap for the two phases. Water and ice clouds do form somewhat separate clusters when $T_4 - T_5$ is plotted against $T_3 - T_4$ (Fig. 4; see also Strabala et al. 1994), but the separation occurs primarily because of the distinct $T_3 - T_4$ differences. What is not shown in Fig. 4 is that the absolute value of $T_4 - T_5$ increases as cloud optical depth decreases. Therefore, large $T_4 - T_5$ differences (positive or negative) indicate thin clouds, water, or ice.

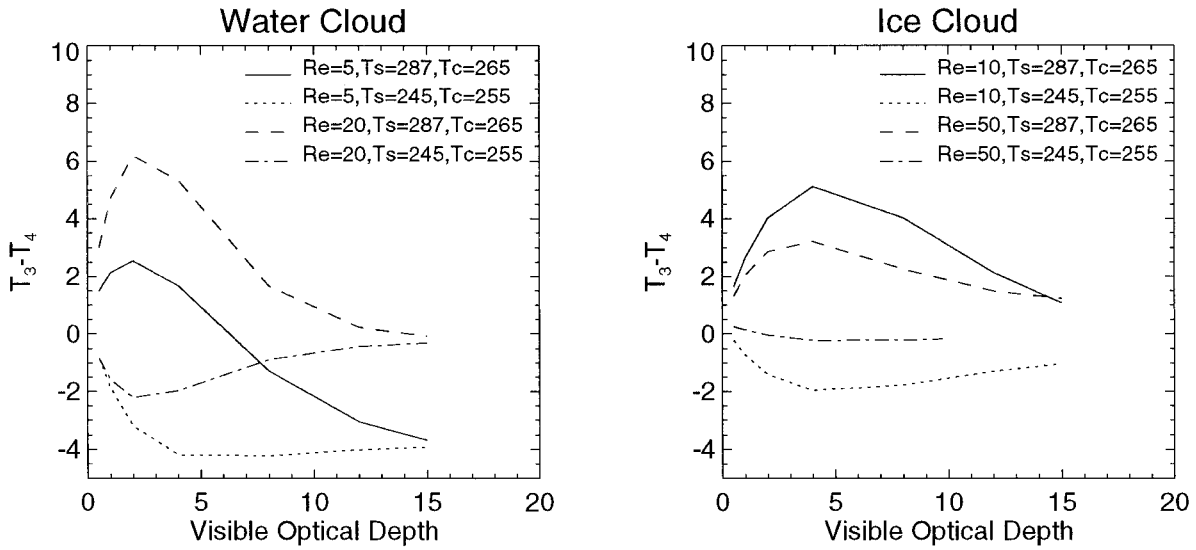

FIG. 3. Modeled AVHRR channels 3 and 4 (3.7 − 11 μm) brightness temperature differences for (left) water and (right) ice clouds. For each of two effective radii, one cold (relative to the surface temperature) and one warm cloud case is given. Calculations were done for midlatitude summer and winter nighttime conditions, with nadir view and a surface emissivity of 0.99.

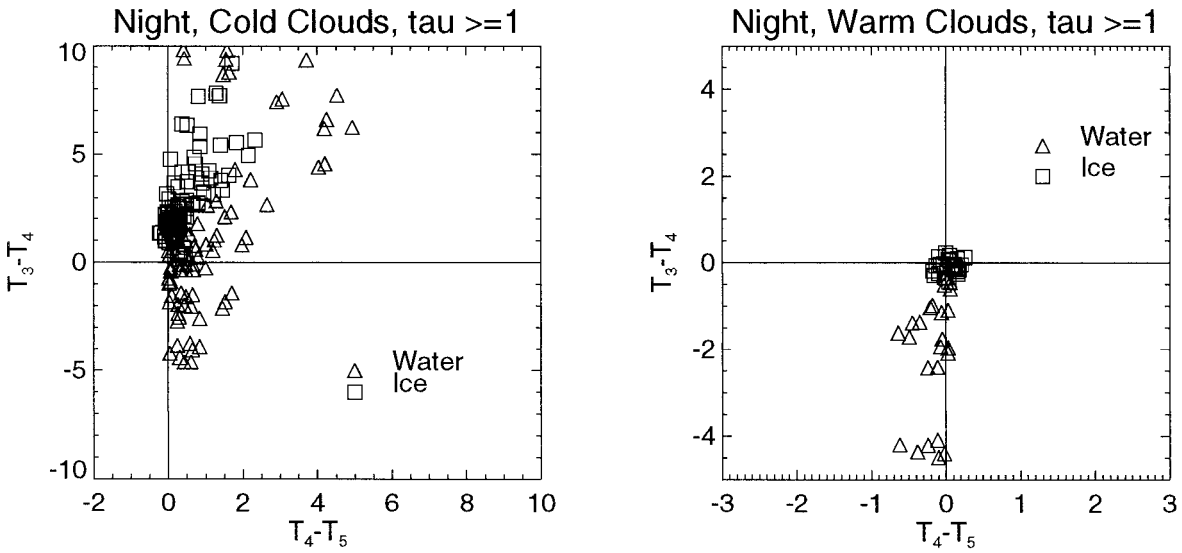

FIG. 4. Modeled brightness temperature differences for AVHRR channels 3 minus 4 (3.7 − 11 μm) and channels 4 minus 5 (11 − 12 μm) for water and ice clouds. The visible optical depth for the data shown is one or greater. Water clouds have top temperatures greater than 250 K; ice clouds are less than 270 K. Calculations were done for tropical, midlatitude, and Arctic conditions over viewing angles from 0° (nadir) to 60°, with a surface emissivity of 0.99.

These theoretical principles give rise to certain relationships that can be used to determine cloud particle phase at night.

1) With cold water cloud, as droplet size decreases, as optical depth τ increases, and as surface temperature T_s approaches the cloud temperature T_c, $T_3 - T_4$ becomes more negative. For example, $T_3 - T_4$ will be less than −2 K if T_s is within 10 K of T_c and $\tau >$ 5. If $T_s - T_c$ is between 15 and 40 K, then τ must be greater than 15 for $T_3 - T_4$ to be less than −2 K.
2) Positive water cloud $T_3 - T_4$ values occur when clouds are thin and $T_s - T_c$ is large and positive.
3) The more negative $T_3 - T_4$ values for water clouds correspond to ice cloud $T_3 - T_4$ values near zero, either negative or positive, for water and ice clouds of a given optical depth.
4) As $T_s - T_c$ increases and is positive, ice cloud $T_3 - T_4$ increases and is positive.
5) Thin clouds have $T_4 - T_5$ values greater than approximately 1.5 K or less than −0.5 K. Water cloud $T_4 - T_5$ values tend to be larger positive or smaller negative than those of ice clouds.

So while ice cloud $T_3 - T_4$ is positive or near zero for both thick and thin clouds, water cloud $T_3 - T_4$ is negative only if the cloud is optically thick or if the surface is significantly colder than the cloud. The value $T_4 - T_5$ can be used to determine if a cloud is optically thin, but it is not a good discriminator of particle phase.

b. Daytime

In the presence of solar radiation, ω at 3.7 μm is the primary spectral feature distinguishing ice and water clouds. Ice particles do not scatter as efficiently as water droplets at this wavelength because of the real part of the index of refraction and the fact that ice clouds are typically composed of larger particles than water clouds. The 3.7-μm reflectance depends not only on particle phase, but also on viewing/illumination geometry and surface reflectance. This is illustrated in Fig. 5, which shows modeled reflectances as a function of the scattering angle. For these daytime model results hexagonal ice crystals were used. In the AVHRR data, the 3.7-μm reflectance is approximated by removing from the total radiance an estimate of the emitted portion based on the temperature of channel 4

$$\rho_3 = \frac{L_3 - B_3(T_4)}{L_0\mu - B_3(T_4)}, \tag{1}$$

where ρ_3 is the channel-3 reflectance, L_3 is the channel-3 radiance, $B_3(T_4)$ is the Planck function for channel 3 based on the channel-4 temperature T_4, L_0 is the solar constant for the band (adjusted for earth–sun distance), and μ is the cosine of the solar zenith angle. The scattering angle ψ is the angle between the incident and reflected beams, defined here as

$$\psi = 180 - \cos^{-1}(\cos\theta_{\text{sun}}\cos\theta_{\text{sat}} + \sin\theta_{\text{sun}}\sin\theta_{\text{sat}}\cos\phi), \tag{2}$$

where θ_{sun} is the solar zenith angle, θ_{sat} is the satellite zenith angle, and ϕ is the relative azimuth angle (where 0 is looking away from the sun and 180 is looking into the sun); all angles are in degrees. As defined in (2), a scattering angle of 0° implies forward scattering; 180° means backscattering. The figure gives reflectances for cloud visible optical depths between 2 and 5, and for

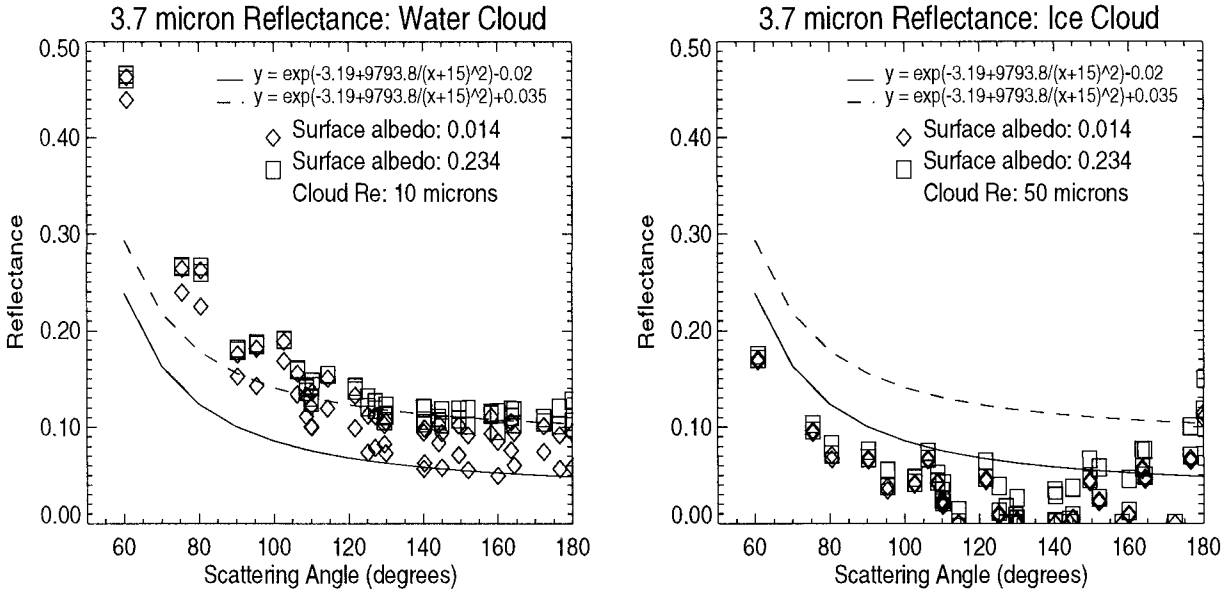

FIG. 5. AVHRR channel 3 (3.7 μm) modeled reflectances as a function of scattering angle for (left) water and (right) ice clouds, and for snow (diamond) and vegetation (square) surfaces. All clouds have visible optical depths in the range 2–15. Also shown are the functions that approximately divide water and ice clouds for each surface type. Calculations were done using midlatitude summer conditions.

snow and vegetation surfaces. These two surface types exhibit very different 3.7-μm clear-sky reflectances, where snow is very dark and vegetation is relatively bright. The smooth curves represent approximate upper limits of ice-cloud reflectance over each surface type, valid for ψ values between 0° and 150°. In the case of strong backscattering ($\psi > 150°$), and in the case of thin clouds over snow, there is no clear separation between water and ice cloud.

The ratio of the 3.7- to 0.6-μm reflectances was also examined, because it provides somewhat better spectral separation of cloud reflectances over the two surface types because of the large difference in visible reflectances. In addition, the relationship between the reflectance ratio and scattering angle becomes nearly linear. However, it provides no additional quantitative information, so simple reflectances are used instead.

3. Procedures

The phase algorithm starts by exploiting the physical property that only ice crystals will exist below some threshold temperature and only liquid droplets will exist above some other threshold temperature. For optically thick clouds the 11-μm brightness temperature will be very close to the kinetic temperature, and simple temperature thresholds can be used to distinguish particle phase. For example, if T_4 were less than some minimum value, for example, $\gamma_{\min} = 243.16$ K (−30°C), then an optically thick cloud would almost certainly be composed of only ice crystals. Similarly, if T_4 were greater than some maximum value, $\gamma_{\max} = 273.16$ K (0°C), then the cloud would be liquid.

However, for optically thin clouds surface emission is a significant part of the measured radiance, and the relationship between the surface temperature T_s and the pixel temperature T_4 must be considered. Using the two thresholds above there are four relationships between the surface temperature and T_4 that can be exploited to determine the phase of clouds that have temperatures less than $\gamma_{\min}$ or greater than $\gamma_{\max}$, as listed in Table 1. The values $\gamma_{\min} = 243.16$ and $\gamma_{\max} = 273.16$ are used in this study.

In practice the clear-sky temperature is used as a proxy for T_s in this step, although T_s under cloud cover will generally be somewhat lower than the clear-sky value during the day (negative cloud radiative effect) and somewhat higher at night. Therefore T_s can be adjusted by a small amount δ. At night we use $\delta = -2$ K and during the day $\delta = +2$ K. Uncertainties in T_s (and δ) of a few degrees should have little effect on the results unless there is a high frequency of clouds with temperatures clustered around the threshold values given in Table 1. If no estimate of T_s is available then an alternate, though less robust, method would be to use simple thresholds; for example, if T_4 is less than 243 K

TABLE 1. Phase assignment based on temperature relationships.

Condition	Phase
$T_s - \delta < \gamma_{\max}$ and $T_4 > \gamma_{\max}$	Liquid
$T_s - \delta > \gamma_{\max}$ and $T_4 > T_s$	Liquid
$T_s - \delta > \gamma_{\min}$ and $T_4 < \gamma_{\min}$	Ice
$T_s - \delta < \gamma_{\min}$ and $T_4 < T_s$	Ice

then the cloud is ice and if T_4 is greater than 303 K then the cloud is liquid. Hutchison et al. (1997b) use -40°C for the lower threshold but suggest that -30°C is probably a reasonable lower bound. They do not suggest an upper bound for liquid clouds.

Application of the four conditions in Table 1 constitutes the first step of phase determination. The tests do not handle water clouds with temperatures less than $\gamma_{\max}$ or less than T_s or ice clouds with temperatures greater than $\gamma_{\min}$ or greater than T_s.

The second step employs the spectral properties described in the previous section and is different for day and night conditions. It is applied to the cloudy pixels that were not labeled in the first step. At night the tests are intended to identify optically thick water cloud and thick ice cloud. The tests are (i) if $T_3 - T_4$ is less than -0.5 K then it is a water cloud and (ii) if $T_3 - T_4$ is greater than $+1$ K and $T_4 - T_5$ is between 0 and 1 K then it is a thick ice cloud.

During the day the tests in the second step utilize the two reflectance functions shown in Fig. 5, which define a threshold ζ between ice and water clouds

$$\zeta = \exp\left(a + \frac{b}{\psi^2}\right) + c, \tag{3}$$

where a, b, and c are coefficients based on modeled reflectances. Only pixels with ψ less than 150° and $T_4 - T_5$ less than 1 K are evaluated, because reflectances for strong backscattering and thin clouds are ambiguous. Observed 3.7-μm reflectances less than the threshold function values are ice cloud; those greater than the function values are water cloud. Surface types other than the snow and vegetation used here should have 3.7-μm reflectances between these two cases. The same functional form can be retained, and the last term (0.035 for vegetation and an implied value of 0 for snow) can be linearly interpolated for other surface types.

The last step, day and night, is to label any pixels that were not handled by the previous two steps. A simple temperature threshold is employed; if the 11-μm brightness temperature is less than 258.16 K (-15°C) then the cloud is ice, otherwise it is liquid. Last, because of the low precision and high uncertainty in the AVHRR T_3 value (and therefore $T_3 - T_4$) when temperatures are very low, all pixels with T_4 less than 230 K are labeled as ice cloud.

4. Limitations

The phase of thin clouds cannot be determined with brightness temperature differences (step 2, night) because $T_3 - T_4$ and $T_4 - T_5$ are nonzero and of the same sign for both phases. If they are very warm or very cold, the temperature tests (step 1) will correctly identify them, but thin water clouds with temperatures less than $\gamma_{\max}$ or less than T_s and thin ice clouds with temperatures greater than $\gamma_{\min}$ or greater than T_s are problematic.

Ice clouds with small particles (less than 10–15 μm) and water clouds with large droplets (greater than 15–20 μm) have similar $T_3 - T_4$ responses (Fig. 3), and therefore are ambiguous in the phase detection procedure (step 2). Fortunately, two physical properties alleviate this problem. First, large droplets and small ice crystals are more common at high and low temperatures, respectively, so they are more likely to be handled by the temperature tests in step 1. Second, typical water droplet effective radii are closer to 10 μm and ice crystal effective radii are commonly in the 30-50-μm range [cf. Rossow et al. (1996) for a description of the ISCCP radiative model, which uses values of 10 μm for water clouds and 30 μm for ice clouds]. Incorrect phase determination for clouds with these ''extreme'' particle sizes is therefore expected to be relatively infrequent.

The phase determination procedures label all cloudy pixels as either ice (solid) or water (liquid). Multilayer and mixed-phase clouds are not identified as such. This problem is particularly apparent in the case of ice cloud over water cloud during the day. If the ice cloud is very cold then the temperature tests (step 1) will label it as ice. Otherwise, it will be labeled as water cloud by the reflectance test. In both cases the result is not incorrect, but is not completely correct either. Incorrect results typically occur in two other situations. Very thin water clouds over snow/ice may be mislabeled during the day because of the low 3.7-μm reflectance of the underlying surface. The same will be true of clouds that occupy only a small proportion of a pixel, as often occurs for cumuliform clouds and at cloud edges.

5. Validation

Validation of the algorithms presented here is performed using two datasets: surface-based lidar depolarization ratios and aircraft measurements of cloud particle characteristics. The Depolarization and Backscatter Unattended Lidar (DABUL) instrument, developed at NOAA's Environmental Technology Laboratory (ETL), was deployed as part of the year-long Surface Heat Budget of the Arctic Ocean (SHEBA) project (Moritz et al. 1993). Daytime and nighttime data over a broad range of illumination and temperature conditions are available. Over the course of the year DABUL documented that liquid water phase was prevalent in the Arctic atmosphere even during the darkest, coldest winter months (Intrieri et al. 1999). The lidar obtained continuous measurements with a range resolution of 30 m and a time resolution of 5 s. The lidar data used in this study were processed for 10-min time averages.

DABUL, which operates at a wavelength of 523 nm, transmits very short pulses of laser light into the atmosphere. A small portion of this energy is scattered back to the system, in two orthogonal polarizations, to yield range-resolved information on cloud and aerosol particle properties (Alvarez et al. 1998). Because the light scattering process depends on the scattering angle

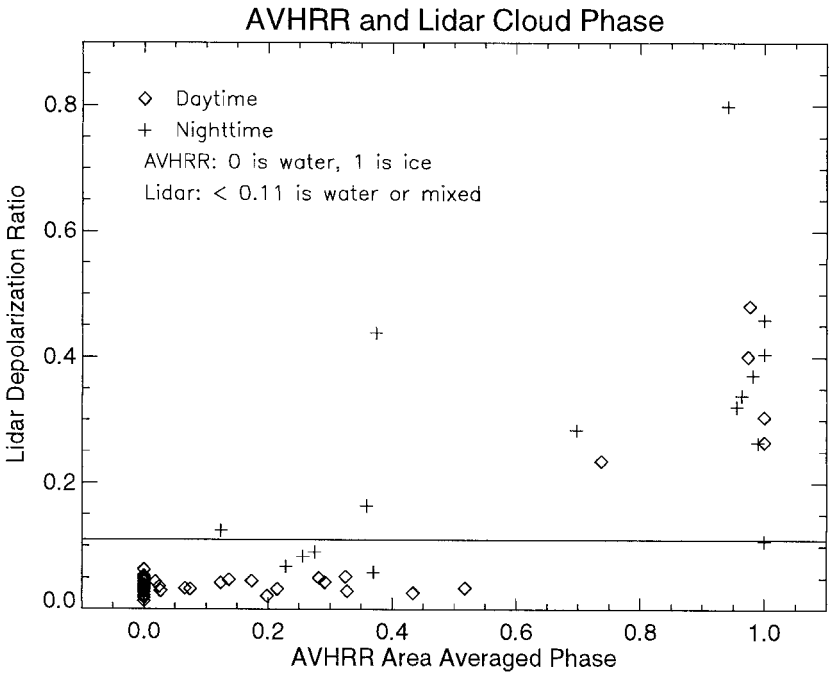

FIG. 6. Cloud particle phase from the AVHRR and lidar depolarization ratio during the SHEBA year. Depolarization ratios less than 0.11 are primarily water or mixed-phase clouds. The AVHRR results use a value of zero for water and one for ice; intermediate values correspond to scenes with both phases present.

as well as the particle shape, size, orientation, and composition we can utilize the lidar polarization backscatter to infer phase. Symmetric (spherical) particles backscatter energy through a combination of axial reflections and/or surface waves that do not change the incident polarization state. The backscatter from complicated shapes (crystalline) induces internal reflections that rotate the incident polarization state resulting in depolarization.

Lidar measurements of cross- and copolarization returns are used to distinguish between the liquid and solid phases of water in the atmosphere. The depolarization ratio is defined as the ratio of the intensity of the received or backscattered light in the perpendicular polarization to the intensity of the backscattered light in the parallel direction. Small raindrops, water-cloud droplets, and fog are considered to be spherical and have depolarization ratios that theoretically approach 0. Nonspherical particles such as ice crystals and snowflakes contain a cross-polarized component produced by internal reflections and refractions and can exhibit depolarization ratios greater than 0.30. Although a variety of laboratory and field studies have been conducted to quantify the depolarization ratios associated with water, mixed-phase, and ice particles, results vary widely. By data point inspection and comparisons with the microwave radiometer liquid water column measurements, it was determined that DABUL depolarization values of less than 0.11 indicate liquid water phase.

The intensity and/or depolarization ratio fields were compared with a threshold to determine cloud base and top heights. Signal-weighted average values of the depolarization ratio for each layer were then calculated. These ratios yielded the associated phase of that layer. It is important to note that lidar signal can attenuate in heavy water-laden clouds. The detection of water occurrence in the column is accurate but the observation of ice cloud above a water cloud may have a negative bias.

Figure 6 gives a comparison of AVHRR-derived cloud phase and lidar depolarization ratio during the SHEBA year. The lidar results are for the highest altitude layer detected. Multilayer, multiphase cases were excluded from the analysis. The AVHRR results for a 50 km $\times$ 50 km area around the lidar location were used, but only for scenes with a cloud fraction of at least 0.6 (60%). Data are once daily at approximately 1400 local solar time. The AVHRR phase labeling is zero for water and one for ice; intermediate values correspond to scenes with both phases present in varying proportions. The figure illustrates that for homogeneous scenes there is almost perfect agreement between the lidar and satellite determinations of phase; that is, all cases labeled as water (ice) cloud by the AVHRR algorithms, day or night, are also labeled as water (ice) cloud by the lidar method. For the cases where the AVHRR algorithm found both phases present but more water than ice cloud—as indicated by an area-average phase value less than 0.5—the lidar cloud type was usu-

ally water. The results for the cases with more ice than water cloud show a similar pattern.

Measurements of cloud particle characteristics by cloud probes on research aircraft can also be used and provide the most direct measurements. The drawbacks to using aircraft data are that flights typically occur during the daytime hours and cloud vertical and horizontal variability and differences between flight times and satellite overpass times result in very few cases that are satisfactory for validation studies. Here we provide very limited validation with only four daytime cases. The validation data are from the Beaufort and Arctic Storms Experiment (BASE) that took place north of Alaska in the fall of 1994 (Curry et al. 1997), and from SHEBA. The National Center for Atmospheric Research C-130 aircraft was used in both experiments. Relatively homogeneous clouds occurred on the following dates: 18 May 1998 (water, optically thick), 3 June 1998 (water, optically thin), 7 June 1998 (ice and water), and 12 October 1994 (mixed-phase cloud). The first three are from SHEBA; the last is from BASE. In the SHEBA cases the particle phase retrievals were completely accurate. For the 18 May case only the 3.7-μm reflectance test (step 2) was needed. For 3 June $T_4 - T_5$ was greater than 1.0 for many pixels so the phase for those pixels was determined only by the T_4 value (step 3), which was 262 K or greater. The 7 June case had some water cloud identified as such by the reflectance test (step 2), and cold ice cloud labeled by the temperature test (step 1). All three tests are therefore useful. The AVHRR retrievals identified the mixed-phase cloud on 12 October as a water cloud because of its high 3.7-μm reflectance.

6. Conclusions

The physical principles underlying the retrieval of cloud particle phase with the AVHRR reflected infrared (3.7 μm) and thermal (11 and 12 μm) channels were described for daytime, nighttime, cold cloud, and warm cloud conditions. It was demonstrated that brightness temperature differences at the three wavelengths and reflectance at 3.7 μm provide necessary, but not sufficient, information for phase determination, and that the relationship between the cloud and surface temperatures must also be considered. Algorithms that utilize these principles were presented and were shown to be accurate for homogeneous phase cloud cases when compared with lidar and aircraft measurements. Although it is clear that the AVHRR does not provide enough spectral information to determine accurately the phase of some thin clouds or to identify multilayer, multiphase cloud systems, the results presented here demonstrate that the instrument can be used for accurate phase determination in general.

Acknowledgments. This work was supported by NASA Grants NAG5-4903 and NAGW-2407, and NSF Grant OPP-9701757. Thanks are due to James Pinto for providing the BASE and SHEBA aircraft data and to Chuck Fowler for the AVHRR dataset.

REFERENCES

Alvarez, R. J., II, W. L. Eberhard, J. M. Intrieri, C. J. Gsund, and S. P. Sandberg, 1998: A depolarization and backscatter lidar for unattended operation in varied meteorological conditions. *Proc., 10th Symp. on Meteor. Observations and Instrumentation,* Phoenix, AZ, Amer. Meteor. Soc., 140–144.

Arking, A., and J. D. Childs, 1985: Retrieval of cloud cover parameters from multispectral satellite images. *J. Climate Appl. Meteor.,* **24,** 322–333.

Baum, B. A., R. F. Arduini, B. A. Wielicki, P. Minnis, and S.-C. Tsay, 1994: Multilevel cloud retrieval using multispectral HIRS and AVHRR data: Nighttime oceanic analysis. *J. Geophys. Res.,* **99**(D3), 5499–5514.

Curry, J. A., J. O. Pinto, T. Benner, and M. Tschudi, 1997: Evolution of the cloudy boundary layer during the autumnal freezing of the Beaufort Sea. *J. Geophys. Res.,* **102**(D12), 13 851–13 960.

Giraud, V., J. C. Buriez, Y. Fouquart, and F. Parol, 1997: Large-scale analysis of cirrus clouds from AVHRR data: Assessment of both a microphysical index and the cloud-top temperature. *J. Appl. Meteor.*, **36,** 664–675.

Heymsfield, A. J., L. M. Miloshevich, A. Slingo, K. Sassen, and D. O'C. Starr, 1991: An observational and theoretical study of highly supercooled altocumulus. *J. Atmos. Sci.,* **48,** 923–945.

Hutchison, K. D., B. J. Etherton, and P. C. Topping, 1997a: Validation of automated cloud top phase algorithms: Distinguishing between cirrus clouds and snow in a priori analyses of AVHRR imagery. *Opt. Eng.,* **36,** 1727–1737.

——, ——, ——, and H. L. Huang, 1997b: Cloud top phase determination from the fusion of signatures in daytime AVHRR imagery and HIRS data. *Int. J. Remote Sens.,* **18,** 3245–3262.

Intrieri, J. M., C. W. Fairall, and B. J. McCarty, 1999: Lidar-derived Arctic cloud properties and radiation measurements during the polar winter season at SHEBA. *Proc. of the Fifth Conf. on Polar Meteorology and Oceanography,* Dallas, TX, Amer. Meteor. Soc., 154–157.

Key, J., 1999: *The Cloud and Surface Parameter Retrieval (CASPR) System for Polar AVHRR.* CIMMS, University of Wisconsin, 59 pp.

——, and A. J. Schweiger, 1998: Tools for atmospheric radiative transfer: Streamer and FluxNet. *Comput. & Geosci.,* **24,** 443–451.

Moritz, R. E., J. A. Curry, N. Untersteiner, and A. S. Thorndike, 1993: Prospectus: Surface heat budget of the Arctic Ocean. NFSF-ARCSS OAII Tech. Rep. 3, 33 pp. [Available from the SHEBA Project Office, Polar Science Center, Applied Physics Laboratory, University of Washington, Seattle, WA 98105.]

Rossow, W. B., A. W. Walker, D. E. Beuschel, and M. D. Roiter, 1996: *International Satellite Cloud Climatology Project (ISCCP) Documentation of New Cloud Datasets.* World Meteor. Org., 115 pp.

Sassen, K., 1991: The polarization lidar technique for cloud research: A review and current assessment. *Bull. Amer. Meteor. Soc.,* **72,** 1848–1866.

Slingo, A., and H. M. Schrecker, 1982: On the shortwave radiative properties of stratiform water clouds. *Quart. J. Roy. Meteor. Soc.,* **108,** 407–426.

Stone, R. S., G. L. Stephens, C. M. R. Platt, and S. Banks, 1990: The remote sensing of thin cirrus cloud using satellites, lidar, and radiative transfer theory. *J. Appl. Meteor.,* **28,** 353–366.

Strabala, K. I., S. A. Ackerman, and W. P. Menzel, 1994: Cloud properties inferred from 8–12-μm data. *J. Appl. Meteor.,* **33,** 212–229.

Yamanouchi, T., K. Suzuki, and S. Kawaguchi, 1987: Detection of clouds in Antarctica from infrared multispectral data of AVHRR. *J. Meteor. Soc. Japan,* **65,** 949–961.